Title: Nicotine-Related Beliefs Induce Dose-Dependent Responses in the Human Brain

Authors: Ofer Perl*[1,2,3], Anastasia Shuster[1,2], Matthew Heflin[1,2], Soojung Na[1,2], Ambereen Kidwai[4], Natalie Booker[5], William C. Putnam[5], Vincenzo G. Fiore[1,2], Xiaosi Gu[1,2,3]*

Affiliations:

[1]Center for Computational Psychiatry, Icahn School of Medicine at Mount Sinai; New York, NY, 10029, USA

[2]Department of Psychiatry, Icahn School of Medicine at Mount Sinai; New York, NY 10029, USA,

[3]Nash Family Department of Neuroscience, Icahn School of Medicine at Mount Sinai; New York, NY, 10029, USA

[4]School of Behavioral and Brain Sciences, University of Texas at Dallas; Dallas, TX, 75080, USA

[5]Department of Pharmacy Practice, Jerry H. Hodge School of Pharmacy; Texas Tech University Health Sciences Center, Dallas, TX, 75235, USA

*Correspondence:
Ofer Perl (O.P) oferikoo@gmail.com, Xiaosi Gu (X.G) xiaosi.gu@mssm.edu.

Abstract (113 words):
Could non-pharmacological constructs, such as beliefs, impact brain activities in a dose-dependent manner as drugs do? Here, nicotine-addicted human participants were made to believe that an electronic cigarette they were about to vape contained either “low”, “medium”, or “high” levels of nicotine, while nicotine strength was held constant. We then measured their brain signals during decision-making with functional MRI. Across the entire brain, we found that only the thalamus, a brain region rich in nicotinic acetylcholine receptors, showed a dose-dependent response to beliefs in both neural activity and connectivity with the prefrontal cortex. These findings demonstrate a dose-response relationship between beliefs and neurobiology, a mechanism previously known to only apply to pharmacological agents.

Introduction

The concept of dose-response comes from pharmacology where the amount of active ingredients in a drug is known to modulate biological processes proportionally (*1*, *2*). In the case of neuropharmacology, establishing dose-response relationships has been fundamental for understanding the biochemical mechanisms mediating drug actions in the human brain. But is it possible that abstract cognitive constructs—such as beliefs—could modulate neurophysiological responses in a similar dose-dependent manner? Cognitive interventions that rely on changing one's beliefs, have been shown to affect brain and behavior (*3*). Still, these non-pharmacological, narrative-based interventions have traditionally been considered qualitative in nature and thus, lacking the measurable precision that is usually required for medicine or biological research.

We hypothesized that human beliefs could modulate neural activities in a dose-dependent fashion that is similar to pharmacologically-induced dose responses. This hypothesis is based on accumulating evidence suggesting that beliefs can interact with human biology. Notable examples include placebo and nocebo effects, in which one's symptoms improve or worsen due to positive ("placebo") or negative beliefs ("nocebo") about a treatment, while the drug contains no active ingredients (*3*). Even in the presence of a powerful neuroactive substance (e.g., nicotine), beliefs about nicotine can exert a binary all-or-none type of effect on neural responses in smokers (*4*). Collectively, these findings support the notion that beliefs can broadly affect neurobiological activities in humans. However, it is unclear whether beliefs can exert a dose-dependent-like effect on the brain. If so, such a finding would reveal a higher degree of sophistication and precision of the interaction between human beliefs and neurobiology than previously understood.

Results

We investigated this question by telling nicotine-addicted human participants that the strength of nicotine contained in an electronic cigarette (e-cig) they were about to vape was either "low", "medium", or "high". This made participants believe that nicotine content differed across e-cigs although the actual nicotine content was in fact kept constant across belief conditions. After vaping, participants (20 participants and a total of 60 scans) performed a monetary decision-making task during functional magnetic resonance imaging (fMRI; **Fig. 1a**). We chose to measure brain signals during reward processing because both nicotine itself and belief about nicotine have been shown to influence reward-related neural activities probed by similar decision-making paradigms (*4*–*7*).

Smokers' self-reported belief about nicotine content increased linearly with engineered belief

We took extensive measures to control for confounding factors. First, participants might vape less in "weaker" nicotine conditions due to a lack of interest. To control for this, we set vaping time to 20 minutes and quantified the amount of nicotine intake by measuring cartridge weight before and after vaping. Nicotine intake—indexed by change in cartridge weight (mg) —did not differ across belief conditions ($F(2,38) = 1.806$, $P = 0.178$; **Fig. 1b**). Second, nicotine metabolism might differ between belief conditions. To address this, we collected saliva samples

both before and after vaping for high-performance liquid chromatography tandem mass spectrometric (LC-MS/MS) analytical quantification of cotinine—a nicotine metabolite indicative of plasma nicotine levels (*8*). Changes in cotinine concentrations (ng/mL) were comparable across conditions ($F(2,32) = 0.959$, $P = 0.393$; **Fig. 1c)**. Third, we measured their exhaled carbon monoxide (CO) before vaping as an index of participants' baseline nicotine saturation level. We did not observe differences in CO levels across conditions (parts per million, ppm; $F(2,32) = 0.364$, $P = 0.698$; **Fig. 1d**). Finally, we examined if participants subjectively believed the instructions by asking them to rate perceived nicotine strength using a 10-point scale. Participants' ratings significantly increased as a function of instructed beliefs (mean ± SD (AU); 'low': = 3.52 ± 0.61, 'medium': = 4.52 ± 0.41, 'high': = 5.82 ± 0.47, $F(2,38) = 9.71$, $P = 0.0004$; **Fig. 1e**). Taken together, these analyses mitigate the concern that imbalanced nicotine consumption, metabolism, or baseline deprivation might have contributed to any neural differences across conditions, while confirming that our instruction successfully influenced participants' beliefs about nicotine strength.

Brain responses for monetary signals in bilateral posterior thalamus increased as a function of belief in a dose-dependent fashion

Next, we examined how instructed beliefs about nicotine might have modulated brain activities during reward-based decision-making in our participants. In a whole-brain analysis of reward-related neural activities, only the thalamus exhibited dose-dependent responses to instructed beliefs about nicotine strength (peak at (-15, -19, -1); family-wise error (FWE) cluster-level corrected $k = 50$, $P = 0.006$; **Fig. 2a**) Region of interest (ROI) analysis using an independent anatomical mask further confirmed this dose-dependent responses in the posterior thalamus (mean ± SD (AU); 'low': = 0.157 ± 1.047, 'medium': = 0.601 ± 0.714, 'high': = 2.914 ± 0.865; standard rmANOVA test $F(2,38) = 3.62$, $P = 0.036$, **Fig. 2b;** permutation test $P = 0.002$, **Fig. 2c)**. Several control analyses confirmed that the identified dose-response in thalamic activation was not due to spatial smoothing (**Supplementary Fig. 1**) or sensorimotor effects (i.e., button press or visual cues; **Supplementary Fig. 2)**. Furthermore, in contrast to the thalamus, the ventral striatum – a region also known to encode nicotine- and reward-related signals – tracked reward activities across all conditions ($P_{FWE} < 0.05$, **Supplementary Fig. 3**), but its responses were not modulated by beliefs (**Supplementary Fig. 4-5**). These results show that across the entire brain, only the thalamus exhibited dose-dependent responses to instructed beliefs about nicotine strength.

Given the individual variability in susceptibility to instructions, we next asked whether participants' subjective beliefs, indexed by their self-reported perception about nicotine strength, also modulated thalamic responses. We found that across all participants and all sessions, subjective ratings of perceived nicotine strength correlated with reward-related activities in the thalamus (Spearman correlation, $r = 0.27$, $P = 0.035$, **Fig. 2d**), suggesting that these brain signals were linked to participants' perceptions about nicotine strength following belief instructions. Taken together, these analyses further confirmed that experimental instructions about nicotine strength shaped subjective perception in our participants and induced dose-dependent neural responses in the thalamus, a brain region with one of the highest concentrations of nicotinic acetylcholine receptors (nAChRs) and a main binding site for nicotine (*9*, *10*).

Belief about nicotine modulated connectivity between prefrontal cortex and thalamus in a dose-dependent manner

At the circuit level, the thalamus is heavily connected to various cortical regions and is known to contribute to higher-order cognition via these connections (*11*). Thus, we hypothesized that belief might also modulate the functional connectivity between the thalamus and higher cortical regions such as prefrontal regions. To this end, we carried out a psychophysiological interaction (PPI ; see Methods) analysis (*12*) to investigate how beliefs about nicotine affected task-related functional connectivity between thalamus and rest of the brain. We found that across the whole brain, belief about nicotine modulated functional connectivity between the thalamus and the ventromedial prefrontal cortex only (vmPFC; peak at (-11, 50, -6), $P_{\text{uncorrected}} < 0.005$, $k = 5$) in a dose-dependent fashion (**Fig. 3a-b**). The vmPFC is a brain region heavily implicated in the computation of value and belief updating (*13*). Thus, this result suggests that in addition to modulating thalamic activation itself, belief about nicotine was also capable of scaling circuit-level interactions between the thalamus and prefrontal regions involving in higher-level cognition and decision-making.

Discussion

Can beliefs impact brain activity in a dose-dependent manner? Here, we found that neural responses in the thalamus varied as a function of belief about nicotinic strength. The thalamus —especially its posterior portion—contains one of the highest densities of nAChRs in the human brain, quantified by both autoradiography (*14*) and functional imaging (*15*). This anatomical feature is hypothesized to account for the attention-enhancing effect of nicotine (*15*), as the thalamus is also known to gate sensory information. Expanding previous work showing acute dose-dependent responses induced by nicotine in the human thalamus (*16*), our finding demonstrates that cognitive constructs such as beliefs and expectations can modulate fine-grained biological mechanisms in the human brain in a way similar to pharmacological agents.

We also found that vmPFC-thalamus connectivity scaled as a function of belief about nicotine strength. The vmPFC has been extensively studied in the context of value-based decision-making processes, and particularly in computing a “common currency” of subjective value (*17*). In serving this role, the vmPFC has been shown to receive input from both the ventral tegmental area and the basal ganglia via the thalamus (*18*). Furthermore, vmPFC-thalamus functional coupling has been shown to subserve expectations about incoming visual stimuli (*19*). Our finding expands previous work by demonstrating that instead of a binary “switch”, the vmPFC-thalamus circuit encodes information related to beliefs and expectations in a dose-dependent manner, highlighting the importance of this circuitry mechanism in high-order cognition.

In sum, this study provides insight into the dose-dependent impact of abstract concepts such as beliefs, on the fronto-thalamic neural circuitry in a manner resembling pharmacological dose-dependent effects. This finding opens up new avenues for systematically leveraging the impact of narratives on the brain in mental health research and treatment.

Materials and Methods

Participants

The study was approved by the Institutional Review Board of the University of Texas at Dallas and the University of the Texas Southwestern Medical Center where data collection was conducted. The sample size was computed by G*Power 3.1.9.7. Assuming a three-measurements repeated-measures ANOVA *F*-test with the effect size of 0.4, alpha of 0.05, and power of 0.95, the minimally required sample size was 18 participants.

Nicotine-dependent adult participants were recruited from the Dallas-Fort Worth (DFW) metropolitan area. Inclusion criteria include an age of 18 years and older, normal or adjusted to normal vision, and smoking a minimum of 10 cigarettes a day for a period exceeding one year but with no prior experience with vaping devices or current attempt to quit smoking. Exclusion criteria included the use of illicit drugs in the past two months, a history of traumatic brain injury, any current substance abuse (excluding nicotine and alcohol), any contraindication to MRI, or previous or current psychiatric, neurological, or major medical conditions. Participants were scanned in accordance with a protocol approved by the UT Dallas and UT Southwestern institutional review boards after providing written consent.

Twenty-three participants enrolled in this study and underwent three fMRI sessions, spaced about one week apart. Three participants were excluded from analysis for the following reasons: one participant was excluded due to software malfunction, one due to falling asleep in the scanner and one due to loss of behavioral data for one of the scanning sessions. The final sample therefore comprised of 20 participants (6 females, age: 41.1± 11.97 years, age range: 24-61 years). Participants were all right-hand dominant.

Experimental design

Upon arrival at the laboratory, participants completed demographic, state (Positive and Negative Affect Schedule, Beck's Depression Inventory, Drug Abuse Screening Test, Short Michigan Alcohol Screening Test, EQ, Toronto Alexithymia Scale, Behavioral Inhibition System and Domain-Specific Risk-Taking questionnaires) and smoking history surveys (Fagerström Test for Nicotine Dependence, Wisconsin Withdrawal Scale, Shiffman-Jarvik Withdrawal scale) . Participants provided saliva samples for measuring cotinine, the primary metabolite of nicotine. Saliva samples were collected using a passive drool method until a volume of 1.8 – 2ml was obtained. They were then coded and stored in designated freezers until sent for analysis. Participants' exhaled carbon monoxide (CO) levels served as proxy for their satiety status. These were acquired by a Smokerlyzer (coVita micro+basic, Santa Barbara, CA) prior to e-cig vaping in each session. The measurement took place in a designated behavioral testing rooms adjacent to the scanners. Participants continuously exhaled through a designated straw until a measurement appeared on screen. For nicotine delivery, we used the Blu e-cig atomizer with disposable cartridges in the 'classic tobacco' flavor. Following the fMRI scans, participants repeated the state-based series of surveys and provided a second saliva sample.

Three participants' data were removed from cotinine analysis: two due to cotinine readings exceeding 3 standard deviations from the mean of the cohort and one due to missing data. Data for all three sessions (instructed belief conditions) were discarded from this analysis. Three participants' data (non-overlapping with the previous omission) were removed from CO

analysis: two due to readings exceeding 3 standard deviations from times the mean of the cohort and one due to missing data. Once again, data for all three sessions (instructed belief conditions) were discarded from this analysis.

Prior to vaping, the e-cig cartridge was weighed three times on a high precision scale and the average of the three measurements was logged as the baseline weight of the cartridge. A similar procedure was done post-vaping and the change in cartridge weight represented the amount of nicotine liquid consumed by the participant. Using a double-blind procedure, neither participants nor the research assistants (M.H. and A.K.) responsible for data collection had prior knowledge about the true nicotine content in the e-cigs. The order of belief conditions was randomly assigned for each participant. The e-cig cartridges were carefully re-labelled as ‘low’, ‘medium’, or ‘high’ by the PI (X.G.) herself to avoid un-blinding by either the participant or the research assistants. Research assistants (M.H. and A.K.) who interacted with the participants adhered to a fixed text during the manipulation stating: “The cartridge you will use today will contain: [mild-to-no nicotine] / [a medium amount of nicotine] / [a high amount of nicotine].” These experimenters also made sure that participants used the e-cig properly, the device was well powered, and that vapor was visible. Participants were told they could vape as much as they wish for the next 20 minutes and were left alone to vape. After 20 minutes they were questioned about any issues with the e-cig. Participants were then prompted to reply how they would rate the strength of the nicotine in the e-cig on a scale of 0 to 10, compared to a normal cigarette.

<u>Cotinine detection in saliva</u>

Chemicals and reagents: Optima LC-MS grade acetonitrile, water and methanol were purchased from Fisher Scientific (New Jersey, USA). Reagent grade ammonium formate was purchased from Sigma Aldrich (Missouri, USA). Cotinine was purchased from Sigma Aldrich. Rac-cotinine-d3 was obtained from Toronto Research Chemicals (Ontario, CAN). All other chemicals and reagents were of analytical grade and used without further purification. Blank human saliva procured from primary investigator. (New York, USA).

Preparation of stock and working solutions of analyte and internal standard: Primary stock solutions of cotinine for the calibration curve (CC) and quality control samples (QC) were prepared from a 1 mg/mL stock solution in methanol. Stock solutions of cotinine were stored at -20 °C, and subsequent dilutions were conducted using water. Primary stock solutions of the bioanalytical method’s internal standard (IS) d3-cotinine were prepared by accurately weighing d3-cotinine and dissolving in methanol to yield a 1 mg/mL stock solution. Stock solutions of d3-cotinine were stored at -20 °C, and subsequent dilutions were conducted using water. For spiking of saliva samples with cotinine, a working stock solution of 1000 ng/mL cotinine in water was prepared and stored at -20 °C. For spiking of saliva samples with d3-cotinine, a working stock solution of 300 ng/mL d3-cotinine in water was prepared and stored at -20 °C.

Preparation of calibration curve and quality control samples for analysis of saliva samples: Cotinine was validated over a calibration range that supports low concentration and high concentration samples. The calibration curve ranged from 5 ng/mL to 1000 ng/mL. Calibration curve samples were prepared by spiking 1µL of the working stock (1 mg/mL cotinine in water) into 250 µL of saliva. This represented the top calibration curve point (i.e., the upper limit of quantification or ULOQ). The remaining calibration curve samples were prepared by serial

dilution of the ULOQ standard in saliva. Quality control were prepared in a similar fashion by spiking 80 µL of the working stock (1000 ng/mL cotinine in water) into 250 µL of plasma. This represented the high-quality control standard (HQC). The medium-quality control standard (MQC) and low-quality control standard (LQC) were prepared by serial dilution of the HQC standard in saliva. Spiking volume of the working standard did not exceed 5% of the matrix volume. QCs for the calibration curve were prepared at 5, 30, and 80 ng/mL.

Saliva Collection: Patients provided a saliva sample collected at various time-points throughout a session. Samples were collected using a passive drool method (i.e., Salimetrics 'SalivaBio' collection aid). Saliva samples were analyzed for cotinine concentrations using a validated LC-MS/MS method.

Saliva Sample Preparation: Acetonitrile (350 µL) and 100 µL (300 ng/mL) d3-cotinine was added to a 250 µL aliquot of saliva. The resultant mixture was centrifuged for 5 min at 5000 rpm at a temperature of 4°C. Five hundred microliters (500µL) of the clear supernatant, was removed, placed in a new Eppendorf tube, and dried using a SpeedVac. Samples were reconstituted using 250 µL of water.

HPLC operating conditions: A Shimadzu CBM-20A Nexera X2 series LC system (Shimadzu Corporation, Kyoto, Japan) equipped with degasser (DGU-20A) and binary pump (LC-30AD) along with auto-sampler (SIL-30AC) and (CTO-30A) column oven. The autosampler was maintained at 15 °C. An injection volume of 1 µL was used and chromatographic separation was achieved using a Kinetex Biphenyl (2.6 µm, 50 × 2.1mm) column. The mobile phase, consisting of 2mM ammonium formate in water (pump A) and methanol:water (95:5) with 0.2% formic acid (pump B) used for the method. The mobile phase pumped using a gradient program at a flow rate of 0.8 mL/min into the mass spectrometer electrospray ionization chamber in positive polarity. Gradient program initiated with 5% of B and maintained for 1.0min, then ramped to 75%B by 2.5min and maintained at 75%B until 3.5min, changed back to 5%B by 4.0min and maintained until 6.01min at the end system controller stop command.
Mass spectrometry operating conditions: Quantitation was achieved employing electrospray ionization in positive ion mode for the analytes using a SCIEX QTRAP 6500+ mass spectrometer (Redwood, CA, USA) equipped with the Turbo V source operated at 550 ºC. The nebulizer gas, auxiliary gas, curtain gas, CAD gas were set at 45, 45, 30 psi and 'medium', respectively. The declustering potential (DP), collision energy (CE), entrance potential (EP) and collision cell exit potential (CXP) were 141, 31, 10, 10 V for (Cotinine-1); 141, 47, 10, 8 V for (Cotinine-2); 141, 31, 10, 12 V for (d3-Cotinine-1); and 141, 29, 10, 8 V for (d3-Cotinine-3), respectively. Detection of the ions was carried out in the multiple-reaction monitoring mode (MRM), by monitoring the precursor > product transitions of 177.0 > 80 and 177.0 > 98.0 (sum over 2 MRMs) for cotinine and 181.2 > 80.1 and 181.2> 101.1 (sum over 2 MRMs) for d3-cotinine. The data obtained were processed by Analyst software™ (version 1.6.3).

Method Validation: The methods for analysis of cotinine in saliva were validated according to the United States FDA's May 2018 Guidance for Industry on 'Bioanalytical Method Validation'. The method was found to have acceptable sensitivity, selectivity, matrix effect, linearity, accuracy, precision, recovery, dilution integrity and stability.

Decision-making task

This task was developed based on a previous investment task (*4*, *5*), but with the modification that participants were allowed to place both positive ('invest') and negative ('short') bets. Briefly, participants were allocated an initial sum of 100 monetary units (i.e., their portfolio) at the beginning of the experiment which could be invested in stock markets. Participants were informed that their final payment would be scaled according to their actual gains or losses in the task. Each participant played a total of 10 markets per visit, each consisting of 20 trials. The stock market prices in the task were chosen from true historical stock market prices. Each task block commenced by a caption titled 'new market' followed by a graphic display of past market dynamics. In each trial *t*, the participant observes the price history of a stock market (including the trial before, p_{t-1}) and places a bet, b_t. Next, a new market price p_t is revealed, and portfolio amounts are updated to reflect the recent outcome. The fractional market return r_t ,is defined as $r_t = (p_t - p_{t-1}) / p_{t-1}$. In each of the 20 trials, participants had unconstrained time to decide on their investment moves. Participants were able to choose to either invest normally (if they think the price will go up) or short sell (if they think the price will go down). Notably, shorting the market would result in gaining from market drops. Thus, people could benefit from either a positive or negative price change and the absolute value of market return $|r_t|$ represents the magnitude of the potential gain. Participants provided their choice using a slider bar and finalized their choice by a button press. Following a 750 ms delay, the new market price was revealed and the fractional change in market price was applied to the portfolio. In later analyses this event is termed 'market reveal'. Each trial concluded in a 750 ms inter-trial interval in which the slider turned gray and became unresponsive. A total of 30 different markets were used across all three visits. Mean session duration in the stock market task was 14.91 ± 3.06 minutes and did not differ across conditions ($F(2,59) = 0.28$, $P = 0.76$).

Image acquisition and preprocessing

Whole-brain anatomical and functional MRI data were acquired on a Philips Achieva scanner with a 3T field strength. High-resolution T1-weighted scans (1.0 × 1.0 × 1.0 mm) were acquired using a 3D magnetization prepared rapid gradient-echo (MPRAGE) sequence. Functional images were acquired using echo-planar imaging (EPI) and tilted 30° from AC-PC axis. The detailed settings for the functional imaging were repetition time (TR) = 2,000 ms, echo time (TE) = 25 ms, flip angle = 90°, voxel size = 3.4 × 3.4 × 4.0 mm, 38 slices. The average number of functional images acquired was 457.37 ± 91.67. All imaging data were preprocessed using standard statistical parametric mapping (SPM12, Wellcome Department of Imaging Neuroscience) algorithms *(fil.ion.ucl.ac.uk/spm).* Functional images were applied a slice time correction.

To account for large head movements often caused by participants' coughing during the scan, we used the ArtRepair toolbox to examine and repair volumes with large motion artifacts. We used the *art_motionregress* and *art_global* modules of the single subject pipeline. The ArtRepair algorithm was further used to generate the motion parameters to be included in the GLM design matrix. Volumes were examined for fast head movements using the automated defaults such that volumes with movement of >0.5 mm/TR were tagged and interpolated with the nearest usable volumes. Overall, 6 out of 60 scans were repaired. The mean functional images for each subject were co-registered to the subject's high-resolution T1 structural scan, using a 12-parameter affine transformation. The participant's T1 image was segmented into gray and white matter and

then normalized using nonlinear basis functions to the Montreal Neurological Institute (MNI) space with the functional images normalized to the template and resampled into 3.4 × 3.4 × 3.4-mm functional voxels. Functional images were smoothed spatially using a 6 mm full-width at half-maximum Gaussian kernel. A temporal high-pass filter of 128 Hz was applied to the fMRI data, and temporal autocorrelation was modeled using a first-order autoregressive function.

Statistical analysis

Throughout this study, we used a within-participant repeated measures ANOVA implemented in MATLAB (*anova_rm*) to assess differences between the three conditions of instructed belief. Normality was assessed with Shapiro-Wilk tests wherever appropriate. During analysis of the various controls if data for one of the sessions was missing, that participant was excluded from this specific analysis.

Behavioral modeling

We carried out linear mixed-effects multiple regression analyses on the series of market returns and investment decisions extracted from each subject. Multiple regression was carried out in R (RStudio 1.1.463, 2018) using the 'lmer' function as follows:

$$|b_{t+1}| \sim 1 + |b_t| + |r_t| + \textit{instructed beliefs} + (\textit{instructed beliefs} * |b_t| \mid \textit{participant})$$

The final return of each market was excluded from the regression, as there is no investment decision following the final market segment. Similarly, the first trial was also removed since it had no preceding investment decision. *P* values were approximated via Satterthwaite's degrees of freedom method. Linear mixed effects were estimated using the full information maximum likelihood (FIML) method.

General linear modeling (GLM) of fMRI data

Event-related analyses of the fMRI data were conducted using SPM12 (Wellcome Department of Imaging Neuroscience). We conducted general linear modeling (GLM) of the functional scans of each participant bey modeling the observed BOLD signals and regressors to identify the relationship between the task events and the hemodynamic response. Regressors related to all visual and motor events were created by convolving a train of delta functions representing the sequence of individual events with the default basis function in SPM12, which consists of a synthetic hemodynamic response function composed of two gamma functions. The GLM included six separate regressors: (1) new market screen display; (2) market history display; (3) all key presses; (4) market price reveal of trial 1; (5) market price reveal of trials 2–19; (6) market price reveal of trial 20. Additionally, six parameters generated during motion correction were entered as covariates. In the GLM, absolute market return $|r|$ was entered as a parametric modulator of market reveal of trials 2–19. We carried out linear contrasts of the parameter estimates to identify the effects in each participant. Statistical maps from all participants were then entered into a second-level group analysis to implement a random-effects statistical model. A within-subject repeated-measures ANOVA model was conducted for the factor of instructed beliefs ('low', 'medium', 'high'). Statistical inference was made based on the F statistics derived from whole-brain rmANOVA statistical maps. Significant effects were identified at the level of $P < 0.005$, with a cluster size threshold of $k = 50$. Maps were rendered using MRIcroGL.

Thalamic parcellation and ROI analyses

We extracted parameter estimates from bilateral thalamus using an anatomical mask (WFU Pick atlas (*20*). Thalamic parcellations were obtained from the Lead-DBS MATLAB toolbox. Each segmented nucleus or region was transformed into the experimental dataset's functional space using the MarsBaR toolbox. The THOMAS (Thalamus optimized multi-atlas segmentation) atlas (*21*) contains 12 non-overlapping nuclei, two of which (MGN and MTT) were too small to be meaningfully transformed to our functional space and were therefore not used. As before, we modeled BOLD activity tracking of fluctuations in magnitude of market return, |r|, and carried out a group analysis with a within-subject rmANOVA design per region of the thalamic parcellation. To account for multiple comparisons, we applied the false-detection rate (FDR) correction to the extracted ROIs at $q = 0.05$.

Permutation analysis

We iteratively shuffled labels for instructed beliefs ('low', 'medium', 'high') within each participant while maintaining their original ratio (i.e., one of each per participant). For each viable permutation (i.e., a permutation whose model estimation converged and yielded any significant voxels), a within-subject rmANOVA was carried out, following which a parameter estimate was derived from the same ROI as the original design matrix to generate a surrogate distribution of beta estimates ($N = 1{,}000$).

Psycho-physiological interaction (PPI) analysis

PPI analysis provides a measure of change in functional connectivity between different brain regions under a specific psychological context (*12*). We defined a seed region – the thalamus – as defined by the WFU anatomical atlas and a psychological context ('market reveal' – the presentation of the investment's return). We then conducted a whole-brain PPI analysis per condition of instructed beliefs and compared those in a within-subject repeated-measures design. The generated PPI model included the PPI term, the physiological regressor, the psychological regressor, and nuisance regressors of six motion parameters. The threshold of significance for the group-level rmANOVA from the PPI regressor was set to be the same as in the GLM ($P < 0.005$) with a cluster size threshold of $k = 5$.

Data availability

Data supporting the findings of this study are deposited in: https://osf.io/3hq6s/

Code availability

The scripts used for data acquisition and analysis are available in: https://osf.io/3hq6s/
Analyses were conducted using open software and toolboxes available online as described in Materials and Methods (SPM: www.fil.ion.ucl.ac.uk/spm/software/spm12; R Studio: https://www.rstudio.com/products/rstudio/download/#download; Lead-DBS: https://www.lead-dbs.org/download/; MRIcroGL: https://www.nitrc.org/projects/mricrogl/)

Acknowledgements
We thank staff members at the UT Southwestern Imaging Center for their assistance with scanning, Jennifer Jung and Mark Labinski for their help with developing the fMRI task, and Jessica Maclin for her help with participant recruitment. We also thank Dr. Laura Berner for her advice on the statistical analysis, and Drs. Daniela Schiller and Paul Kenny for their helpful discussions and comments on the manuscript.

Author Contributions
Conceptualization: XG.
Methodology: OP, AS, NB, WCP, XG
Investigation: MH, SN, AK
Visualization: OP
Funding acquisition: XG
Project administration: MH, XG
Supervision: XG
Writing – original draft: OP, WCP, VGF, XG
Writing – review and editing: OP, VGF, XG

Competing interests
The authors declare that they have no competing interests.

Funding
National Institute on Drug Abuse grant R01DA043695 (XG)
National Institute on Drug Abuse grant R21DA049243 (XG)
University of Texas, Dallas internal funding (XG)
Mental Illness Research, Education, and Clinical Center at the James J. Peter Veterans Affairs Medical Center grant MIRECC VISN 2 (VGF)

Additional information
Supplementary Text
Figs. S1 to S7
Tables S1

References
1. N. D. Volkow, M. Morales, The Brain on Drugs: From Reward to Addiction. *Cell*. **162**, 712–725 (2015).
2. E. R. Korpi, B. den Hollander, U. Farooq, E. Vashchinkina, R. Rajkumar, D. J. Nutt, P. Hyytiä, G. S. Dawe, *Pharmacol. Rev.*, in press, doi:10.1124/pr.115.010967.
3. T. D. Wager, J. K. Rilling, E. E. Smith, A. Sokolik, K. L. Casey, R. J. Davidson, S. M. Kosslyn, R. M. Rose, J. D. Cohen, Placebo-induced changes in FMRI in the anticipation and experience of pain. *Science*. **303**, 1162–1167 (2004).
4. X. Gu, T. Lohrenz, R. Salas, P. R. Baldwin, A. Soltani, U. Kirk, P. M. Cinciripini, P. R. Montague, Belief about nicotine selectively modulates value and reward prediction error signals in smokers. *Proc. Natl. Acad. Sci. U. S. A.* **112**, 2539–2544 (2015).

5. T. Lohrenz, K. McCabe, C. F. Camerer, P. R. Montague, Neural signature of fictive learning signals in a sequential investment task. *Proc. Natl. Acad. Sci. U. S. A.* **104**, 9493–9498 (2007).
6. P. H. Chiu, T. M. Lohrenz, P. R. Montague, Smokers' brains compute, but ignore, a fictive error signal in a sequential investment task. *Nat. Neurosci.* **11**, 514–520 (2008).
7. X. Gu, T. Lohrenz, R. Salas, P. R. Baldwin, A. Soltani, U. Kirk, P. M. Cinciripini, P. R. Montague, Belief about nicotine modulates subjective craving and insula activity in deprived smokers. *Front. Psychiatry*. **7**, 1–11 (2016).
8. G. O. Petersen, C. E. Leite, J. M. Chatkin, F. V. Thiesen, Cotinine as a biomarker of tobacco exposure: Development of a HPLC method and comparison of matrices. *J. Sep. Sci.* **33**, 516–521 (2010).
9. S. Wonnacott, Presynaptic nicotinic ACh receptors. *Trends Neurosci.* **20**, 92–98 (1997).
10. D. Paterson, A. Nordberg, Neuronal nicotinic receptors in the human brain. *Prog. Neurobiol.* **61**, 75–111 (2000).
11. G. M. G. Shepherd, N. Yamawaki, Untangling the cortico-thalamo-cortical loop: cellular pieces of a knotty circuit puzzle. *Nat. Rev. Neurosci.* **22**, 389–406 (2021).
12. K. J. Friston, C. Buechel, G. R. Fink, J. Morris, E. Rolls, R. J. Dolan, Psychophysiological and Modulatory Interactions in Neuroimaging. *Neuroimage*. **6**, 218–229 (1997).
13. M. F. S. Rushworth, T. E. J. Behrens, Choice, uncertainty and value in prefrontal and cingulate cortex. *Nat. Neurosci.* **11**, 389–397 (2008).
14. D. P. Spurden, J. A. Court, S. Lloyd, A. Oakley, R. Perry, C. Pearson, R. G. L. Pullen, E. K. Perry, Nicotinic receptor distribution in the human thalamus: Autoradiographical localization of [3H]nicotine and [125I]α-bungarotoxin binding. *J. Chem. Neuroanat.* **13**, 105–113 (1997).
15. N. S. Lawrence, T. J. Ross, E. A. Stein, Cognitive mechanisms of nicotine on visual attention. *Neuron*. **36**, 539–548 (2002).
16. E. A. Stein, J. Pankiewicz, H. H. Harsch, J. Cho, S. A. Fuller, R. G. Hoffmann, M. Hawkins, S. M. Rao, P. A. Bandettini, A. S. Bloom, Nicotine-Induced Limbic Cortical Activation in the Human Brain : A Functional MRI Study. *Am. J. Psychiatry*. **155**, 1009–1015 (1998).
17. P. W. Glimcher. D.J. Levy, Root of all value. *Changes*. **29**, 997–1003 (2012).
18. S. N. Haber, B. Knutson, The reward circuit: Linking primate anatomy and human imaging. *Neuropsychopharmacology*. **35**, 4–26 (2010).
19. G. Barbalat, N. Bazargani, S.-J. Blakemore, The Influence of Prior Expectations on Emotional Face Perception in Adolescence. *Cereb. Cortex*. **23**, 1542–1551 (2012).
20. J. A. Maldjian, P. J. Laurienti, R. A. Kraft, J. H. Burdette, An automated method for neuroanatomic and cytoarchitectonic atlas-based interrogation of fMRI data sets. *Neuroimage*. **19**, 1233–1239 (2003).
21. J. H. Su, F. T. Thomas, W. S. Kasoff, T. Tourdias, E. Y. Choi, B. K. Rutt, M. Saranathan, Thalamus Optimized Multi Atlas Segmentation (THOMAS): fast, fully automated segmentation of thalamic nuclei from structural MRI. *Neuroimage*. **194**, 272–282 (2019).
22. W. Schultz, P. Dayan, P. R. Montague, A Neural Substrate of Prediction and Reward. *Science.* **275**, 1593–1599 (1997).

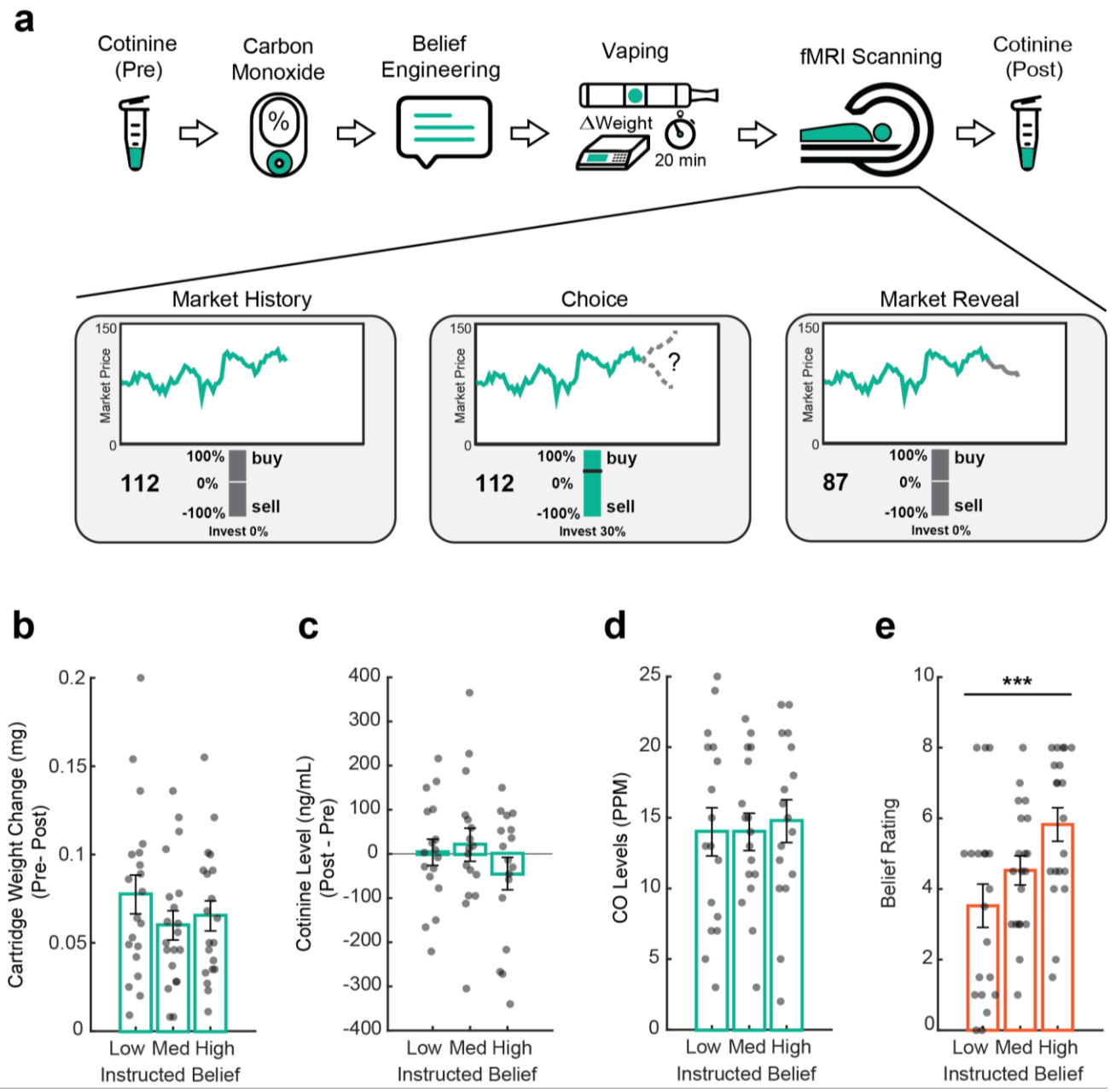

Fig. 1. Experimental paradigm and sanity check measures. (**a**) Participants completed three visits. In each, we collected saliva samples for cotinine measurement, measured carbon monoxide (CO) levels, instructed beliefs, and measured brain activities using fMRI as participants engaged in a decision-making task. (**b**) Change in cartridge weight (pre – post) (P = 0.178), (**c**) cotinine concentration (P = 0.393), or (**d**) CO level (P = 0.698) did not differ between conditions. (**e**) Effect of instructed beliefs on self-reported belief about nicotine strength (P = 0.0004). Bars depict group means and points represent participants. Error bars are SEM. ***P < 0.001.

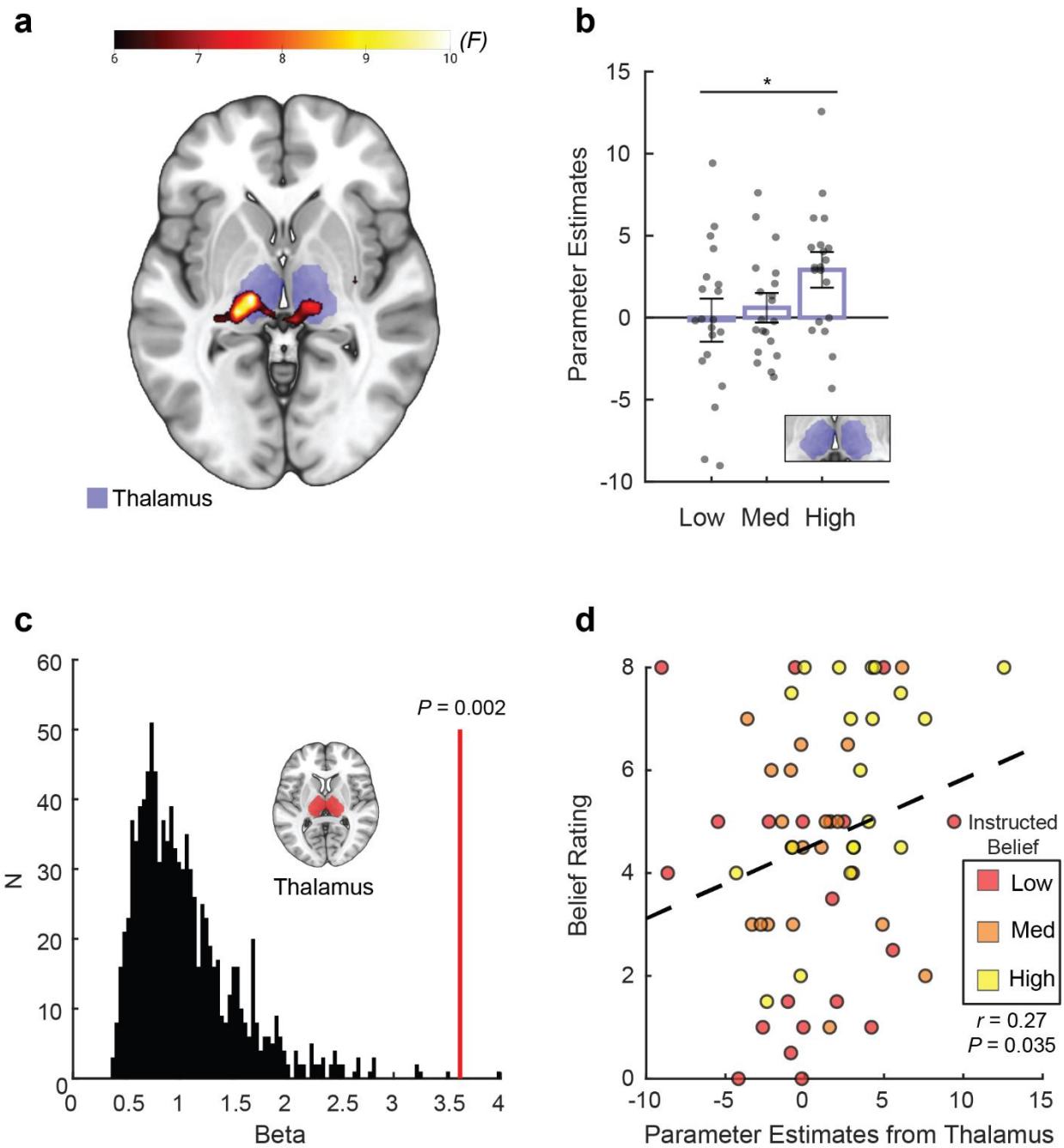

Fig. 2. Belief about nicotine strength induced dose-dependent responses in the thalamus. (**a**) Whole-brain effects of instructed beliefs about nicotine on value-tracking signals (cluster-level P_{FWE} = 0.006, k = 50). (**b**) Parameter estimates representing reward-related activities extracted from an independent thalamus mask (shown in purple) across belief conditions (P = 0.036). Bars depict group means, points represent participants. Error bars are SEM. *P < 0.05. (**c**) Permutation analysis for instructed beliefs conditions (N = 1,000, P = 0.002). A histogram comprised of surrogate distribution for beta estimates (black bars). Red line denotes mean of true

beta values. (**d**) Correlation between thalamic signals and subjective belief rating regarding perceived nicotine strength (r = 0.27, *P* = 0.035). Black dashed line is linear fit.

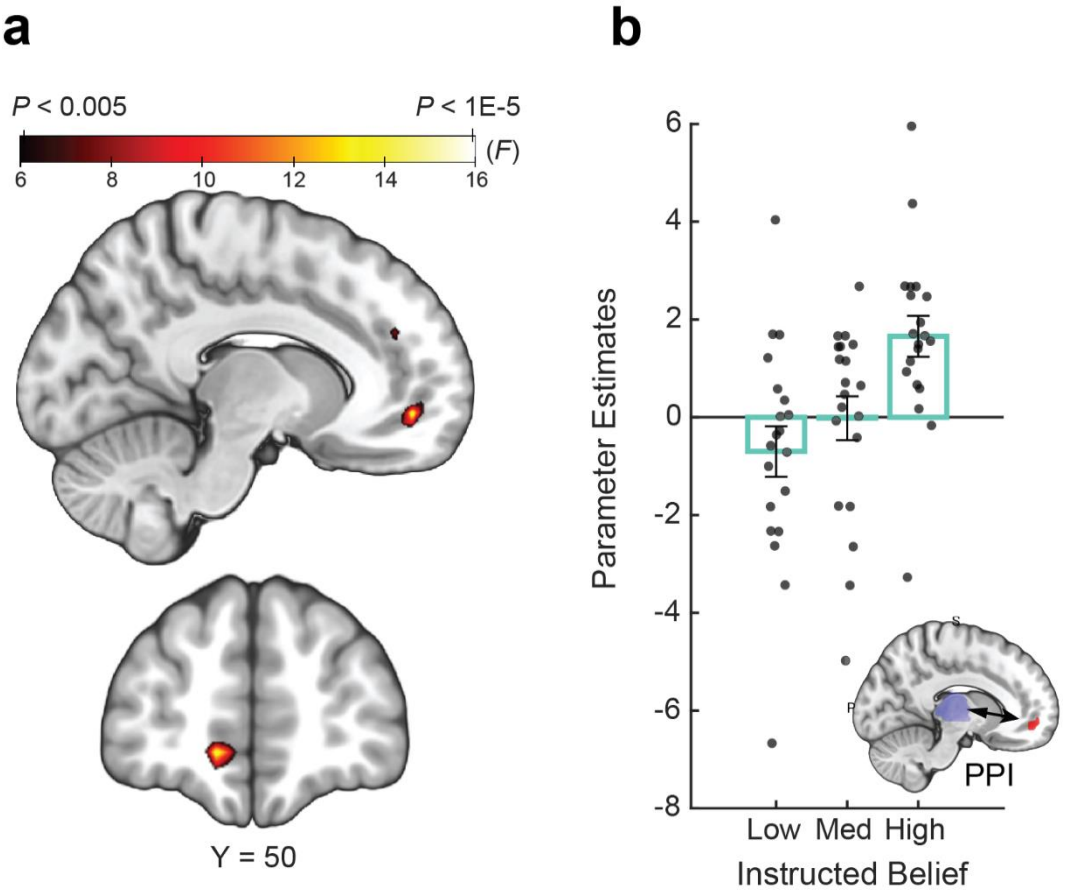

Fig. 3. Belief about nicotine strength modulated thalamus-vmPFC functional connectivity in a dose-dependent fashion. (**a**) Whole-brain effects of instructed beliefs on the psychophysiological interaction (PPI) between the thalamus and rest of the brain (*P* < 0.005, uncorrected, k = 5). (**b**) Parameter estimates extracted from (a) representing functional coupling strength between the thalamus and vmPFC. Bars depict group means, points represent participants. Error bars are SEM.